Localized strain sensing with fiber Bragg-grating ring cavities

C. E. Campanella,[1] A. Giorgini,[2] S. Avino,[2] P. Malara,[2,*] R. Zullo,[2] G. Gagliardi,[2] and P. De Natale[2]

[1]*Consiglio Nazionale delle Ricerche, Istituto di Tecnologie Industriali e Automazione (ITIA) Via Paolo Lembo 38F – 70124 Bari, Italy*

[2]*Consiglio Nazionale delle Ricerche, Istituto Nazionale di Ottica (INO), via Campi Flegrei, 34 - Comprensorio A. Olivetti, 80078 Pozzuoli (Naples), Italy*

[*]*pietro.malara@ino.it*

Abstract: We report the theoretical description and the experimental demonstration of an optical resonator formed by inserting a Fiber Bragg Grating (FBG) in a closed fiber loop. The spectral characteristics of such a resonator strongly depend on the reflectivity of the FBG. In the wavelength region where the FBG reflectivity *R* is negligible, the system behaves like a conventional ring resonator. On the other hand, when *R* is not vanishing, a split-mode structure can be observed, associated to the degeneracy removal of two counterpropagating resonant modes. The magnitude of the mode splitting can be used to sense small variations of the FBG physical parameters, such as length, temperature or group index. An example of strain sensing with this setup is reported, showing that the mode splitting is sensitive to a mechanical strain applied to the FBG, while it is almost insensitive to a strain applied to any other point of the resonator. This peculiar feature allows to perform cavity-enhanced, local strain measurements with a reduced sensitivity to environmental perturbations, which represents an important improvement in the framework of the fiber-optic sensors.

OCIS codes: (230.0230) Optical devices; (230.5750) Resonators; (120.4820) Optical systems.

References and links

1. G. Gagliardi, M. Salza, S. Avino, P. Ferraro, and P. De Natale, "Probing the ultimate limit of fiber-optic strain sensing," Science **330**(6007), 1081–1084 (2010).
2. S. Avino, A. Giorgini, M. Salza, M. Fabian, G. Gagliardi, and P. De Natale, "Evanescent-wave comb spectroscopy of liquids with strongly dispersive optical fiber cavities," Appl. Phys. Lett. **102**(20), 201116 (2013).
3. C. Ciminelli, C. M. Campanella, F. Dell'Olio, C. E. Campanella, and M. N. Armenise, "Label-free optical resonant sensors for biochemical applications," Prog. Quantum Electron. **37**(2), 51–107 (2013).
4. C. Ciminelli, C. E. Campanella, and M. N. Armenise, "Optimized design of integrated optical angular velocity sensors based on a passive ring resonator," J. Lightwave Technol. **27**(14), 2658–2666 (2009).
5. G. Gagliardi, M. Salza, P. Ferraro, P. De Natale, A. Di Maio, S. Carlino, G. De Natale, and E. Boschi, "Design and test of a laser-based optical-fiber Bragg-grating accelerometer for seismic applications," Meas. Sci. Technol. **19**(8), 085306 (2008).
6. T. T.-Y. Lam, G. Gagliardi, M. Salza, J. H. Chow, and P. De Natale, "Optical fiber three-axis accelerometer based on lasers locked to π phase-shifted Bragg gratings," Meas. Sci. Technol. **21**, 094010 (2010).
7. J. E. Heebner, V. Wong, A. Schweinsberg, R. W. Boyd, and D. J. Jackson, "Optical transmission characteristics of fiber ring resonators," IEEE J. Quantum Electron. **40**(6), 726–730 (2004).
8. J. M. Choi, R. K. Lee, and A. Yariv, "Ring fiber resonators based on fused-fiber grating add-drop filters:application to resonator coupling," Opt. Lett. **27**(18), 1598–1600 (2002).
9. F. Vollmer and P. Fischer, "Frequency-domain displacement sensing with a fiber ring-resonator containing a variable gap," Sens. Actuators A Phys. **134**(2), 410–413 (2007).
10. A. Yariv, "Universal relations for coupling of optical power between microresonators and dielectric waveguides," Electron. Lett. **36**(4), 321 (2000).
11. J. Čtyroký, I. Richter, and M. Sinor, "Dual resonance in a waveguide coupled ring micro-resonator," Opt. Quantum Electron. **38**(9–11), 781–797 (2006).

#196218 - $15.00 USD Received 21 Aug 2013; revised 8 Oct 2013; accepted 10 Oct 2013; published 21 Nov 2013

12. C. Ciminelli, C. E. Campanella, F. Dell'Olio, and M. N. Armenise, "Fast light generation through velocity manipulation in two vertically-stacked ring resonators," Opt. Express **18**(3), 2973–2986 (2010).
13. C. Ciminelli, C. E. Campanella, and M. N. Armenise, "Structural polarization conversion in integrated optical vertically stacked ring resonators," Opt. Laser Technol. **48**, 294–301 (2013).

1. Introduction

Fiber Bragg Gratings (FBGs) and Fiber Ring resonators are well-established optical devices widely utilized for their simple manufacturing, small dimensions, low cost and immunity to the EM radiation. FBGs and ring resonators are used in innumerable applications, ranging from telecommunications to physical, chemical and inertial sensing [1–6].

An experimental investigation of the spectral characteristics of fiber ring resonators has been reported in [7], focussing the attention on the power transfer characteristics in the undercoupled, critically coupled and overcoupled regimes. The advantage shown by these resonators consists in the possibility of obtaining tunable optical delay lines without requiring a high finesse by cascading different rings. In [8] a fiber ring optical resonator, formed by adiabatic fused-FBG couplers, has been proposed to control the coupling efficiency (via the grating strength) to switch the device into the three above mentioned operative regimes. In [9] the possibility of carrying out strain-free displacement measurements has been proposed by adopting a fiber ring containing a gap.

In this paper, we theoretically describe and experimentally demonstrate a novel fiber-optic strain sensor obtained by inserting a FBG in a closed fiber loop. The proposed sensing mechanism shows a cavity-enhanced sensitivity to a strain localized in the FBG region while being substantially insensitive to perturbations that affect the rest of the fiber loop.

FBG loop configuration

The optical fiber resonator configuration (see Fig. 1) is made by closing a conventional single-mode silica fiber which includes a FBG in a ring geometry using two fused fiber couplers.

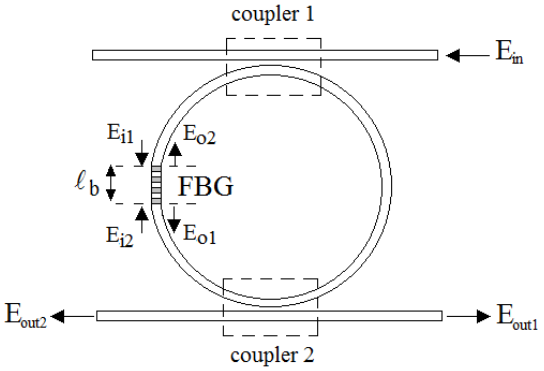

Fig. 1. Sketch of the FBG optical fiber ring resonator.

As shown in Fig. 1, a linearly polarized optical field from a laser source (E_{in}) is launched through the optical fiber in order to excite the resonator modes via the evanescent coupler 1. A photodiode is placed at one of the ends of coupler 2 to monitor the cavity spectral response $\left|E_{out1,2}\right|^2$. Each coupler is modelled as a lumped element by the following transfer matrix, having a unitary determinant if the insertion loss is neglected [10]:

$$\begin{pmatrix} E_{o1c} \\ E_{o2c} \end{pmatrix} = \begin{pmatrix} \tau & -jk \\ -jk & \tau \end{pmatrix} \begin{pmatrix} E_{i1c} \\ E_{i2c} \end{pmatrix} \tag{1}$$

#196218 - $15.00 USD Received 21 Aug 2013; revised 8 Oct 2013; accepted 10 Oct 2013; published 21 Nov 2013

where E_{i1c}, E_{i2c} are the input amplitudes of the coupler and E_{o1c}, E_{o2c} are the coupler outputs. τ and k are the fractions of the optical amplitudes transmitted and coupled by the evanescent coupler, respectively. The FBG is also modelled via a transfer matrix [8]:

$$\begin{pmatrix} E_{o1} \\ E_{o2} \end{pmatrix} = \begin{pmatrix} t & -r \\ -r & t \end{pmatrix} \begin{pmatrix} E_{i1} \\ E_{i2} \end{pmatrix} \tag{2}$$

where E_{i1}, E_{i2} are the amplitudes of the electric fields entering the FBG and E_{o1}, E_{o2} are those of the electric fields exiting the FBG (see Fig. 1). t and r are the fractions of the optical field amplitudes transmitted and reflected via the FBG, respectively, and they are linked through the unitary determinant of Eq. (2), analogously to τ and k in Eq. (1). Being the FBG a dispersive element, t and r can be expressed as [8]:

$$t = \frac{\Theta}{\Theta \cosh\left(\Theta \ell_b\right) + j\Delta\beta \sinh\left(\Theta \ell_b\right)} \tag{3a}$$

$$r = \frac{jK \sinh\left(\Theta \ell_b\right)}{\Theta \cosh\left(\Theta \ell_b\right) + j\Delta\beta \sinh\left(\Theta \ell_b\right)} \tag{3b}$$

where ℓ_b is the length of the FBG, while Θ, K and $\Delta\beta$ can be expressed as functions of the effective fiber refractive index n, the FBG index modulation depth Δn and its central wavelength λ_b in the following way [8]:

$$\Theta = \sqrt{K^2 - \Delta\beta^2}; K = \frac{\pi \Delta n}{\lambda_b}; \Delta\beta = \beta - \frac{2\pi n}{\lambda_b}; \beta = \frac{2\pi n}{\lambda} \tag{4}$$

The total resonator length L is given by the sum of ℓ_b and the remaining fiber length ℓ, respectively. The spectral response, T of the proposed device can be derived by utilizing the matrix formalism of [11]:

$$T = \left|\frac{E_{01}}{E_{in}}\right|^2 = \frac{1}{4}\left|\frac{k^2 e^{-j\beta\frac{L}{2}} a(t+r)}{1-\tau^2 e^{-j\beta L} a^2 (t+r)} + \frac{k^2 e^{-j\beta\frac{L}{2}} a(t-r)}{1-\tau^2 e^{-j\beta L} a^2 (t-r)}\right|^2 \tag{5}$$

where $a = e^{-\alpha L/2}$ is the overall attenuation in the length $L/2$ due to the loss α per unit length. The right hand side of Eq. (5) is a combination of two solutions with opposite phases, which are commonly referred to as "symmetric" and "antisymmetric" modes.

To describe the physical behaviour of this system, a simulation of the transmission spectrum was performed. It is shown in Fig. 2 along with the reflectivity curve of the FBG for wavelengths close to λ_b. In the spectral regions where $r \sim 0$ (left side of Fig. 2), the intracavity power circulates only in the direction of excitation (transmission is only detectable at the output port 1), and the symmetric and antisymmetric solutions of Eq. (5) coincide. In this case, referred to as "degenerate mode condition" [12], the device behaves as a conventional ring resonator. In the spectral region where $r \neq 0$ instead, part of the intracavity power is scattered by the FBG and excites a counterpropagating mode. The subsequent redistribution of the intracavity power leads to a reduction of the signal detected at the output port 1. The non-vanishing R also removes the degeneracy of the symmetric/antisymmetric solutions in Eq. (5), giving rise to a transmission spectrum with split resonant modes [12]. The magnitude of the mode splitting in the non-degenerate mode condition is directly related to the reflectivity of the FBG, and can be expressed, in analogy to the case of a waveguide microresonator [11], as:

#196218 - $15.00 USD Received 21 Aug 2013; revised 8 Oct 2013; accepted 10 Oct 2013; published 21 Nov 2013

$$S_\lambda \approx \frac{\lambda^2}{\pi nL}\frac{|r|}{t} = \frac{\lambda^2}{\pi nL}\sqrt{\frac{R_\lambda}{1-R_\lambda}} \tag{6}$$

Being $\frac{\lambda^2}{\pi nL}$ the Free Spectral Range (FSR) of the resonator in nm and $R_\lambda = |r|^2$ the reflectivity of the FBG at the interrogating wavelength λ.

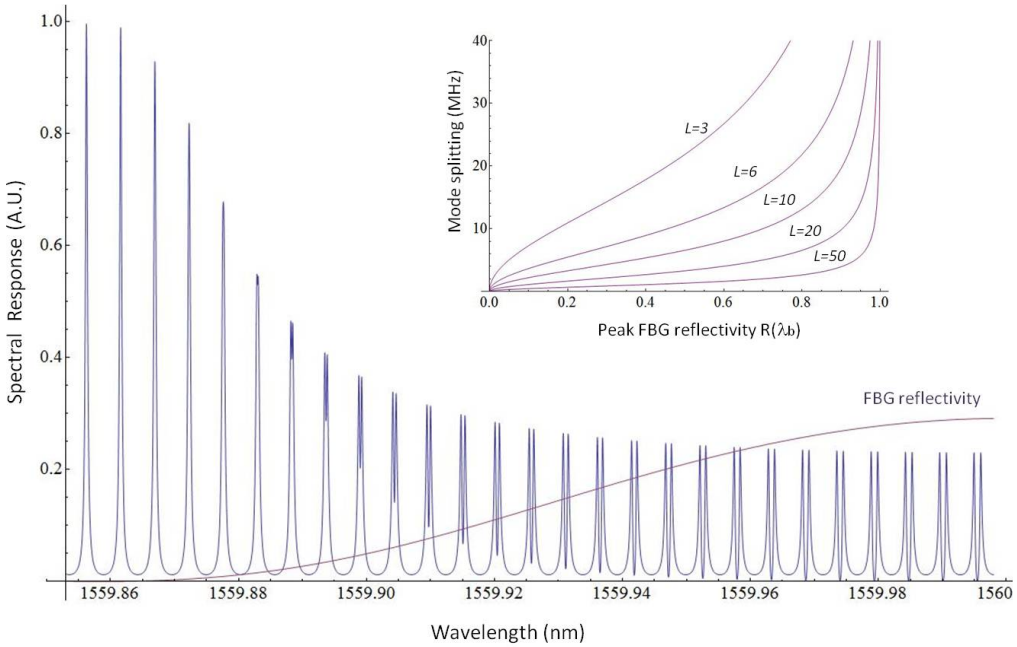

Fig. 2. Simulated spectral response of the FBG ring resonator. As the reflectivity of the FBG increases, the spectrum moves from the degenerate to the non-degenerate mode condition, where split modes can be observed. For ease of illustration, the following parameters were adopted in the simulation: n = 1.457, $\Delta n = 5\cdot 10^{-5}$, λ_b = 1560 nm, λ_b = 0.006 m, λ = 0.3 m, $\alpha = 3.45\cdot 10^{-5}$ m^{-1}, and two fiber couplers with τ = 0.894 (20% coupling efficiency). *Inset*: maximum mode splitting as a function of the peak FBG reflectivity (Eq. (6)) for different cavity lengths.

The FBG loop as a strain sensor

It is easy to see from Eq. (5) and Fig. 3 that the system can transition from the degenerate to the non-degenerate mode by varying the FBG reflectivity. Since the latter is a function of $\lambda - \lambda_b$, this can be done by either tuning the laser across the FBG reflectivity curve, or by shifting the central Bragg wavelength. The amount of splitting of a resonance can thus be used to sense a variation of the FBG physical parameters.

We now consider in particular a perturbation of the cavity length ΔL. Like in any resonator, the variation of the FSR causes any resonance at wavelength λ to shift by an amount $\Delta\lambda = 0.79\lambda\frac{\Delta L}{L}$, where 0.79 is the photoelastic coefficient of the fiber [12]. According to Eq. (6), a variation of the resonance splitting ΔS_λ is also associated to ΔL. In this respect, it is interesting to note that S_λ scales inversely with the overall cavity length $L = \ell_b + \ell$, but also contains an implicit dependence on ℓ_b alone, through the reflectivity R_λ. The same perturbation can then result in different values of ΔS_λ, depending on whether it

#196218 - $15.00 USD Received 21 Aug 2013; revised 8 Oct 2013; accepted 10 Oct 2013; published 21 Nov 2013

affects ℓ or ℓ_b. The sensitivity of S_λ in these two cases can be obtained by differentiating Eq. (6) separately with respect to $\delta\varepsilon = \frac{\delta\ell}{L}$ and $\delta\varepsilon_b = \frac{\delta\ell_b}{L}$.

$$\frac{\partial S_\lambda}{\partial \varepsilon} = -\frac{\lambda^2}{\pi n L}\sqrt{\frac{R_\lambda}{1-R_\lambda}} = -S_\lambda \tag{7a}$$

$$\frac{\partial S_\lambda}{\partial \varepsilon_b} = -S_\lambda + \frac{\lambda^2}{2\pi n}\frac{1}{\sqrt{R_\lambda\left(1-R_\lambda\right)^3}}\frac{\partial R_\lambda}{\partial \ell_b} \tag{7b}$$

Equation (7a) describes the sensitivity of the splitting to a generic strain of the resonator length, which is proportional to the magnitude of initial splitting S_λ. However, if the strain applied involves the FBG length ℓ_b, an additional term appears, associated to the change of the reflectivity R_λ caused by the shift of the Bragg wavelength, as shown by Eq. (7b). It is important to notice that this term is independent of L, whereas S_λ scales inversely with it. Therefore, for a sufficiently long fiber loop, the splitting is only sensitive to local perturbations of the FBG length. This is a crucial advantage with respect to a traditional cavity with Bragg mirrors [1], where none of the observables available (transmitted power or resonance shift) can distinguish the strain applied to a specific point along the resonator.

It is also interesting to notice that, unlike conventional cavity-based strain sensors, the sensitivity to variation of the FBG length depends on the reflectivity curve of the grating itself. To optimize the sensor, the terms on the right hand side of Eq. (7b) must be considered. In particular, $\frac{\partial R_\lambda}{\partial \ell_b} = \frac{\partial R_\lambda}{\partial \lambda_b}\frac{\partial \lambda_b}{\partial \ell_b} = \frac{\partial R_\lambda}{\partial \lambda_b}0.79\lambda_b\frac{\Delta\ell_b}{\ell_b}$ describes the overall response of the FBG reflectivity to a variation of its length. Its value increases for smaller ℓ_b and/or a narrower reflectivity curve. The factor $\frac{1}{2\sqrt{R_\lambda\left(1-R_\lambda\right)^3}}$ instead points out that the sensitivity is higher for either an extremely small or high FBG reflectivity. The optimal working point of the sensor is then a tradeoff between the maximum slope of the reflectivity curve and the maximum/minimum value of R_λ.

2. Experimental setup and results

The theoretical predictions on the described strain sensing mechanism were experimentally demonstrated using the setup shown in Fig. 3. The coherent radiation source is a narrow linewidth fiber laser (Koheras Adjustik) with center wavelength 1560.10 nm and a power of 42 mW, modulated by a ramp generator to visualize the cavity modes. The polarization state of the laser is controlled by a Lefevre-ring controller in order to minimize cavity resonances associated with the excitation of orthogonal polarization states [13]. The ring cavity is formed by using an FBG (measured reflectivity of 15%, Reflection Bandwidth 800 pm and insertion loss of 2.7 dB) integrated in a Single Mode Fiber (SMF) loop having ℓ = 5.98 m (FSR = 34.4 MHz). Radiation is injected in the ring resonator by means of two fiber couplers with 5% efficiency and an insertion loss of 0.2 dB. The signal exiting the FBG ring cavity is detected by a photodiode and visualized on a digital oscilloscope.

#196218 - $15.00 USD Received 21 Aug 2013; revised 8 Oct 2013; accepted 10 Oct 2013; published 21 Nov 2013

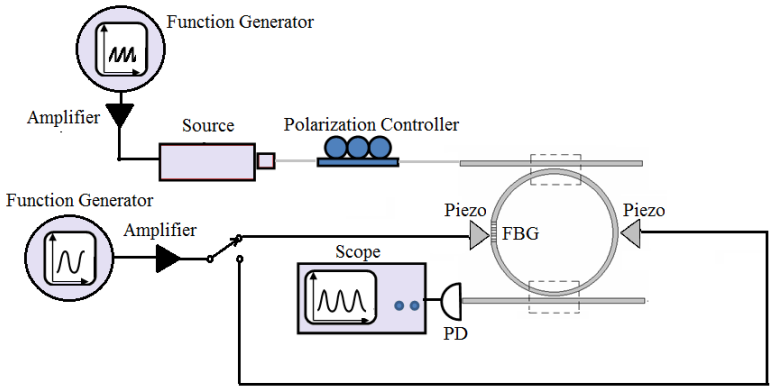

Fig. 3. Experimental setup.

In a first instance, the laser source was tuned at the edge of the non-degenerate region of the spectrum, which represent the starting point of our measurements. Then, a strain ε_b was applied to the intracavity FBG by a piezoelectric transducer, as sketched in Fig. 3, in the direction of increasing splitting. A minimum strain of 25 nε was necessary to achieve a measurable mode splitting (1.4 MHz). Smaller splitting magnitudes are in fact hard to resolve because of the finite linewidth of the cavity resonances. A few examples of transmission spectra obtained for discrete values of the piezo voltage are reported in Fig. 4. The amount of strain corresponding to the different voltages was calculated from the resonance shifts $\Delta\lambda = 0.79\lambda\varepsilon_b$, also visible in Fig. 4.

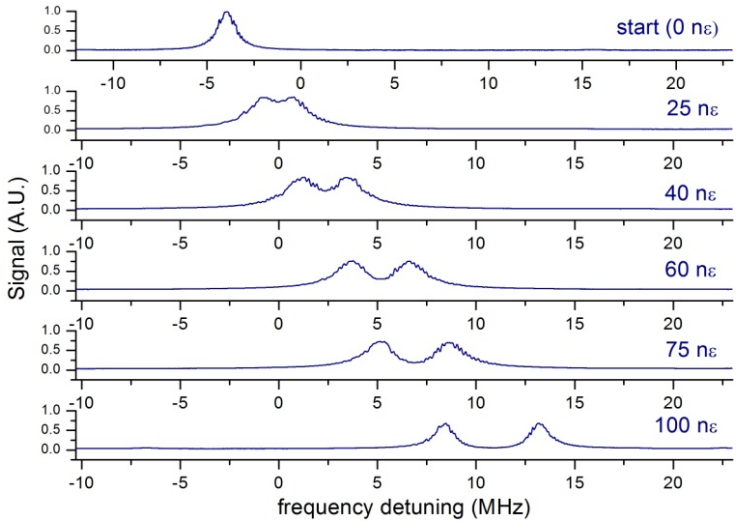

Fig. 4. Resonance splitting and shift for different strains applied to the intra-cavity FBG.

In a second step, we applied an equivalent strain ε to a point of the fiber loop far from the FBG. To do so, voltages producing the same shifts of the interrogated cavity resonance were sent to another piezoelectric transducer (see Fig. 3). The splitting magnitudes associated to equivalent values of strain applied to the FBG and to the fiber loop are plotted in Fig. 5 along with the corresponding theoretical curves.

#196218 - $15.00 USD Received 21 Aug 2013; revised 8 Oct 2013; accepted 10 Oct 2013; published 21 Nov 2013

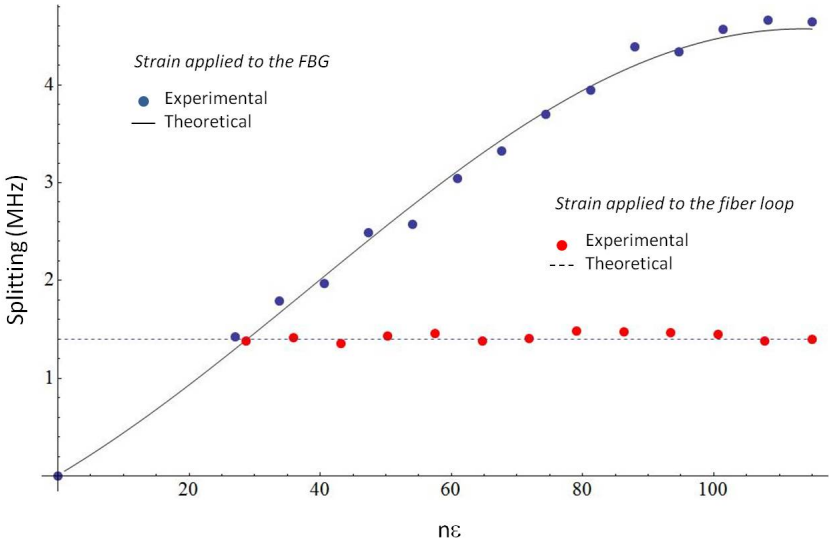

Fig. 5. Splitting magnitude variation measured when the strain is applied to the intracavity FBG (blue points) or to the fiber loop (red points). The theoretical trends from Eq. (6) are plotted along with the experimental data.

To calculate the latter, the grating was previously interrogated with a broadband spontaneous emission source (ASE). Its reflectivity curve was recorded with an optical spectrum analyzer and fitted to a theoretical model to retrieve the FBG parameters $R_0 = 0.15$, $\ell_b = 6$ mm and $\Delta n = 3.4 \cdot 10^{-5}$. These values were then substituted in Eqs. (3) and (6) to plot the theoretical curves of Fig. 5, that perfectly matches the experimental data.

The results above reported clearly show that the resonance splitting is only sensitive to variations of the FBG parameters and in fact immune from perturbations affecting all the rest of the resonator. This demonstrates the possibility to use the described scheme to measure small mechanical deformations, temperature or refractive index variations of the FBG with a cavity enhanced sensitivity and a reduced noise level. The resolution (i.e. the minimum detectable strain) of the demonstrated sensor depends on the ability to resolve the resonant wavelengths of the split modes, and therefore is ultimately limited by the finite linewidth of the cavity resonances (spectral resolution). However, the sensitivity of the splitting measurement can be improved by acting on the FBG parameters, as shown by Eq. (7b). With an optimized FBG design an overall resolution in the order of a few nε can be readily achieved, even with the current spectral resolution.

In conclusion, we have presented a theoretical description of a fiber Bragg grating enclosed in a fiber loop resonator, verified experimentally the model predictions and demonstrated that the device can be used to sense a localized strain applied to the FBG with a sensing mechanism immune to environmental perturbations of the fiber length. We believe that this simple scheme has strong potential for spectroscopic-based strain sensing with FBGs and may find several applications in the fields of opto-mechanics, quantum optics, physics of light-matter interactions and many others.

Acknowledgements

This work was funded by Italian Ministry of Education and Research (MIUR) in the framework of PON01_01209 “BACKOP” project. We thank G. Notariale for technical assistance.

#196218 - $15.00 USD Received 21 Aug 2013; revised 8 Oct 2013; accepted 10 Oct 2013; published 21 Nov 2013